J. Fluid Mech. (1999), *vol.* 387, *pp.* 227–254. Printed in the United Kingdom

Natural convection flow far from a horizontal plate

By VALOD NOSHADI AND WILHELM SCHNEIDER†

Institute of Fluid Dynamics and Heat Transfer, Technical University of Vienna, Wiedner Hauptstrasse 7/322, A-1040 Vienna, Austria

(Received 12 December 1996 and in revised form 7 December 1998)

Plane and axisymmetric (radial), horizontal laminar jet flows, produced by natural convection on a horizontal finite plate acting as a heat dipole, are considered at large distances from the plate. It is shown that physically acceptable self-similar solutions of the boundary-layer equations, which include buoyancy effects, exist in certain Prandtl-number regimes, i.e. $0.5 < Pr \leqslant 1.470588$ for plane, and $Pr > 1$ for axisymmetric flow. In the plane flow case, the eigenvalues of the self-similar solutions are independent of the Prandtl number and can be determined from a momentum balance, whereas in the axisymmetric case the eigenvalues depend on the Prandtl number and are to be determined as part of the solution of the eigenvalue problem. For Prandtl numbers equal to, or smaller than, the lower limiting values of 0.5 and 1 for plane and axisymmetric flow, respectively, the far flow field is a non-buoyant jet, for which self-similar solutions of the boundary-layer equations are also provided. Furthermore it is shown that self-similar solutions of the full Navier–Stokes equations for axisymmetric flow, with the velocity varying as $1/r$, exist for arbitrary values of the Prandtl number.

Comparisons with finite-element solutions of the full Navier–Stokes equations show that the self-similar boundary-layer solutions are asymptotically approached as the plate Grashof number tends to infinity, whereas the self-similar solution to the full Navier–Stokes equations is applicable, for a given value of the Prandtl number, only to one particular, finite value of the Grashof number.

In the Appendices second-order boundary-layer solutions are given, and uniformly valid composite expansions are constructed; asymptotic expansions for large values of the lateral coordinate are performed to study the decay of the self-similar boundary-layer flows; and the stability of the jets is investigated using transient numerical solutions of the Navier–Stokes equations.

1. Introduction

The flow generated by natural convection at large distances from a body acting as a heat source or sink is known as a plume. Several investigations with well documented results (Gebhart *et al.* 1988) have shown that the behaviour of laminar plumes at large Grashof numbers is independent of the details of the flow near the source or sink. It is the net amount of heat transferred to, or from, the fluid, i.e. the heat source or sink strength, that governs the plume. For vertical plumes the buoyancy forces act in the main flow direction, with the result of no pressure variation across the boundary layer.

† Author to whom correspondence should be addressed.

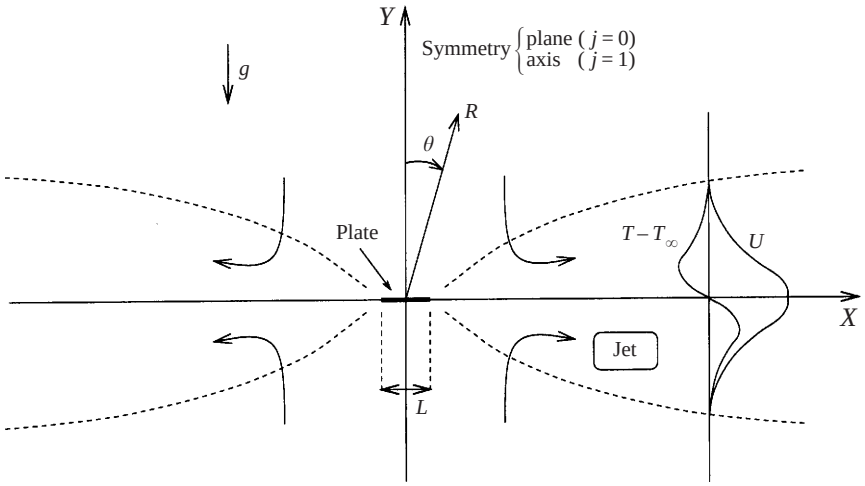

FIGURE 1. Far flow field: plane ($j = 0$) or axisymmetric ($j = 1$) flow.

The flow behaviour is quite different, however, if the body acts as a heat dipole. Suppose the temperatures of the lower and upper surfaces of a finite horizontal plate, as shown in figure 1, are $T_\infty + \Delta T$ and $T_\infty - \Delta T$, respectively, where T_∞ is the constant ambient temperature and ΔT is a positive constant. Provided the thermal expansivity β is positive, the flow is directed from the centre of the plate towards the edges at both the upper and lower surfaces. Provided the symmetry of the flow field corresponds to the symmetry of the boundary conditions (see Appendix C for a discussion of this assumption), the amount of heat transferred from the fluid to the plate at the upper surface is equal to the amount of heat transferred from the plate to the fluid at the lower surface. Thus, where the surface streams merge, a horizontal jet flow develops. This horizontal jet has an antisymmetric temperature profile, which gives rise to rather unusual buoyancy effects that govern the far flow field.

Various similarity solutions for buoyancy-driven horizontal flow problems are known from the literature. Stewartson (1958) and Gill, Zeh & Del Casal (1965) provided self-similar solutions to the boundary-layer equations for indirect natural convection flows on horizontal surfaces. Goldshtik & Shtern (1990) found self-similar solutions to the Navier–Stokes equations for axisymmetric free convection near a thermal quadrupole. The properties of non-buoyant plane jets, with a total flow rate of zero, were studied by Goldshtik, Hussain & Shtern (1991).

It is the aim of the present work to investigate the flow field at large distances from a body, in particular a horizontal plate, acting as a heat dipole as described above. The plate length (for plane flow) or the plate diameter (for axisymmetric flow) are denoted by L. The coordinate system X, Y is shown in figure 1, with the Y-axis representing the plane, or axis, of symmetry. The horizontal and vertical velocity components are denoted by U and V, respectively. Alternatively, a polar coordinate system R, θ, see figure 1, with associated velocity components V_r, V_θ, is also used in the course of the analysis. The Boussinesq approximation is applied, and dissipation is neglected in the energy balance. Then the non-dimensional parameters governing the flow are the Prandtl number Pr and the plate Grashof number Gr, i.e.

$$Pr = \frac{\nu}{\alpha} \quad \text{and} \quad Gr = \frac{g\beta\Delta T L^3}{\nu^2}, \tag{1.1}$$

with ν, α and $\beta > 0$ being the constant values of kinematic viscosity, thermal diffusivity and thermal expansivity, respectively, while g denotes the gravity acceleration.

The following non-dimensional variables are introduced:

$$\hat{x} = X/L, \quad \hat{y} = Y/L, \quad \hat{r} = R/L, \tag{1.2a}$$

$$\hat{u} = U/U_{ref}, \quad \hat{v} = V/U_{ref}, \quad \hat{v}_r = V_r/U_{ref}, \quad \hat{v}_\theta = V_\theta/U_{ref}, \tag{1.2b}$$

$$\hat{\Theta} = (T_\infty - T)/\Delta T, \quad \hat{p} = P/\rho_\infty U_{ref}^2, \tag{1.2c}$$

where $U_{ref} = (g\beta\Delta T L)^{1/2}$ is a reference velocity, T and P are the absolute temperature and the pressure, respectively, and ρ_∞ is the constant ambient density. Thus the non-dimensional basic equations for plane ($j = 0$) or axisymmetric ($j = 1$) flow are the continuity equation

$$\frac{\partial(\hat{u}\hat{x}^j)}{\partial\hat{x}} + \frac{\partial(\hat{v}\hat{x}^j)}{\partial\hat{y}} = 0, \tag{1.3a}$$

the Navier–Stokes equations

$$\hat{u}\frac{\partial\hat{u}}{\partial\hat{x}} + \hat{v}\frac{\partial\hat{u}}{\partial\hat{y}} = -\frac{\partial\hat{p}}{\partial\hat{x}} + Gr^{-1/2}\left[\frac{\partial^2\hat{u}}{\partial\hat{x}^2} + \left(\frac{1}{\hat{x}}\frac{\partial\hat{u}}{\partial\hat{x}}\right)^j - \left(\frac{\hat{u}}{\hat{x}^2}\right)^j + \frac{\partial^2\hat{u}}{\partial\hat{y}^2}\right], \tag{1.3b}$$

$$\hat{u}\frac{\partial\hat{v}}{\partial\hat{x}} + \hat{v}\frac{\partial\hat{v}}{\partial\hat{y}} = -\frac{\partial\hat{p}}{\partial\hat{y}} + Gr^{-1/2}\left[\frac{\partial^2\hat{v}}{\partial\hat{x}^2} + \left(\frac{1}{\hat{x}}\frac{\partial\hat{v}}{\partial\hat{x}}\right)^j + \frac{\partial^2\hat{v}}{\partial\hat{y}^2}\right] - \hat{\Theta}, \tag{1.3c}$$

and the energy equation

$$\hat{u}\frac{\partial\hat{\Theta}}{\partial\hat{x}} + \hat{v}\frac{\partial\hat{\Theta}}{\partial\hat{y}} = \frac{Gr^{-1/2}}{Pr}\left[\frac{\partial^2\hat{\Theta}}{\partial\hat{x}^2} + \left(\frac{1}{\hat{x}}\frac{\partial\hat{\Theta}}{\partial\hat{x}}\right)^j + \frac{\partial^2\hat{\Theta}}{\partial\hat{y}^2}\right]. \tag{1.3d}$$

It is to be expected that, under certain conditions, the flow field possesses properties of self-similarity. Thus, in §§ 2 and 3, we seek self-similar solutions to the boundary-layer equations, both with and without buoyancy effects, depending on the value of the Prandtl number. In § 4 a particular, self-similar solution to the full equations of motion will be given. Finally a comparison of numerical and analytical solutions (§ 5) will not only lend support to the results but also provide further insight into the characteristics of the far flow field. Further, and more detailed, results can be found in Noshadi (1996).

2. Horizontal buoyant jets

2.1. *Boundary-layer equations and self-similarity*

We consider here self-similar, buoyancy-affected far fields for large Grashof numbers. Subject to *a posteriori* justification it is assumed that the flow of interest resembles a horizontal slender jet flow, see figure 1. Thus the governing equations are the boundary-layer equations

$$\frac{\partial(ux^j)}{\partial x} + \frac{\partial(vx^j)}{\partial y} = 0, \tag{2.1}$$

$$u\frac{\partial u}{\partial x} + v\frac{\partial u}{\partial y} = -\frac{\partial}{\partial x}\int_y^\infty \Theta\,\mathrm{d}y + \frac{\partial^2 u}{\partial y^2}, \tag{2.2a}$$

$$u\frac{\partial \Theta}{\partial x} + v\frac{\partial \Theta}{\partial y} = \frac{1}{Pr}\frac{\partial^2 \Theta}{\partial y^2}, \tag{2.2b}$$

$$v = \frac{\partial u}{\partial y} = \Theta = 0 \quad \text{at} \quad y = 0, \tag{2.3a}$$

$$u = \Theta = 0 \quad \text{as} \quad y \to \infty \tag{2.3b}$$

in terms of the scaled non-dimensional variables

$$x = \hat{x}, \quad y = \hat{y}Gr^{1/5}, \tag{2.4a}$$

$$u = \hat{u}Gr^{1/10}, \quad v = \hat{v}Gr^{3/10}, \quad \Theta = \hat{\Theta}. \tag{2.4b}$$

The first term on the right-hand side of the momentum equation (2.2*a*) accounts for the pressure variation due to buoyancy forces (cf. Gersten & Herwig 1992 or Gebhart *et al.* 1988).

The continuity equation (2.1) is satisfied with the help of a stream function ψ, i.e.

$$u = x^{-j}\frac{\partial \psi}{\partial y}, \quad v = -x^{-j}\frac{\partial \psi}{\partial x}. \tag{2.5}$$

Defining the similarity variables η, f and ϑ according to the relationships

$$y = c\, x^{\lambda_1}\eta, \quad \psi = c^{-1}x^{\lambda_2}f(\eta), \quad \Theta = c^{-5}x^{\lambda_3}\vartheta(\eta), \tag{2.6}$$

where c is an arbitrary free constant, and introducing the dummy variable $q(\eta) = \int_\infty^\eta \vartheta \, \mathrm{d}\eta$, transforms the basic equations (2.1) and (2.2*a*, *b*) into the following set of ordinary differential equations:

$$q' - \vartheta = 0, \tag{2.7a}$$

$$f''' + \lambda_2 f f'' - (1 - 2\lambda_1)f'^2 - \lambda_1 \eta \vartheta + 2(1 - 2\lambda_1)q = 0, \tag{2.7b}$$

$$\vartheta'' + Pr\left(\lambda_2 f \vartheta' - \lambda_3 f' \vartheta\right) = 0, \tag{2.7c}$$

provided the exponents λ_1, λ_2 and λ_3 satisfy the relationships

$$\lambda_2 = (1 + j) - \lambda_1, \quad \lambda_3 = 2 - 5\lambda_1. \tag{2.8}$$

Since (2.6) contains the free constant c, the value of $f'(0)$ can be normalized to 1 without loss of generality. Herewith the boundary conditions become

$$f = f' - 1 = f'' = \vartheta = 0 \quad \text{at} \quad \eta = 0, \tag{2.9a}$$

$$q = f' = \vartheta = 0 \quad \text{as} \quad \eta \to \infty. \tag{2.9b}$$

2.2. *Integral conservation laws*

Integrating the momentum equation (2.7*b*) from zero to infinity and making use of the boundary conditions (2.9*a*, *b*) gives

$$(2 + j - 3\lambda_1)\int_0^\infty f'^2 \mathrm{d}\eta + (2 - 3\lambda_1)\int_0^\infty \eta\vartheta \, \mathrm{d}\eta = 0. \tag{2.10}$$

Since $f'^2 > 0$ and $\vartheta > 0$, both integrals in (2.10) are positive. In the plane flow case, i.e. $j = 0$, the coefficients of both integrals are equal to $(2 - 3\lambda_1)$, with the result that the exponent λ_1 must have the constant value

$$\lambda_1 = \tfrac{2}{3} \quad (\text{for} \quad j = 0). \tag{2.11}$$

This is the same value as for the classical plane jet. Thus the momentum flow is conserved, i.e.

$$\frac{\mathrm{d}}{\mathrm{d}x}\int_0^\infty u^2 \mathrm{d}y = 0 \quad (\text{for} \quad j = 0). \tag{2.12}$$

Since, in the case of plane flow, λ_1 is determined solely from similarity requirements and integral conservation considerations, the corresponding solution is a self-similar solution of the first kind according to Barenblatt (1979).

In the axisymmetric flow case, however, equation (2.10) requires that the coefficients of the integrals have different signs. To satisfy this condition it is not necessary that λ_1 has a definite value. It is sufficient that λ_1 is in the interval

$$\tfrac{2}{3} < \lambda_1 < 1 \quad (\text{for} \quad j = 1)\,. \tag{2.13}$$

Thus, in the axisymmetric flow case, λ_1 is an eigenvalue that is to be determined from solving the set of equations (2.7*a–c*), (2.8) and (2.9*a*, *b*) with Pr as a parameter. In the notation of Barenblatt (1979), this results in a self-similar solution of the second kind.

2.3. *Solutions for plane flow*

It is possible to integrate the momentum equation (2.7*b*) with $\lambda_1 = \frac{2}{3}$ once, reducing the original set of equations (2.7*a–c*) to

$$q' - \vartheta = 0, \tag{2.14a}$$

$$3f'' + ff' - 2\eta q = 0, \tag{2.14b}$$

$$\frac{3}{Pr}\vartheta'' + f\vartheta' + 4f'\vartheta = 0, \tag{2.14c}$$

with the boundary conditions

$$f = f' - 1 = \vartheta = 0 \quad \text{at} \quad \eta = 0; \tag{2.15a}$$

$$q = f' = 0 \quad \text{as} \quad \eta \to \infty. \tag{2.15b}$$

The set of nonlinear ordinary differential equations was solved numerically with a B-spline collocation method at Gaussian points (Ascher, Christiansen & Russel 1981). There were three collocation points at each interval, and the boundary values were prescribed at both ends.

A solution was found for any Prandtl number, figures 2 to 4, with a singularity at $Pr = Pr^* = 1.470588 = 25/17$. Note that there are reversed flow regions due to buoyancy effects (figure 2).

As Pr approaches the critical value Pr^*, $f(\infty)$ vanishes, see figure 4, indicating that entrainment into the jet becomes zero. As a consequence, the decay of both velocity and temperature disturbances as $\eta \to \infty$ is algebraic for $Pr = Pr^*$, while it is of the common exponential type if $Pr \neq Pr^*$, see Appendix B. This behaviour resembles the limit solutions of the boundary-layer equations as investigated by Brown & Stewartson (1965).

For $Pr > Pr^*$ the entrainment is again positive, but the temperature disturbance profiles, as shown in figure 3, contain regions of negative values, which implies that the mathematical solution for $Pr > Pr^*$ is unlikely to describe a real natural convection flow in an infinite domain.

As $Pr \to \frac{1}{2}$, the reversed flow region and the temperature disturbance vanish such that at $Pr = \frac{1}{2}$ the solution is identical to the solution of the classical isothermal

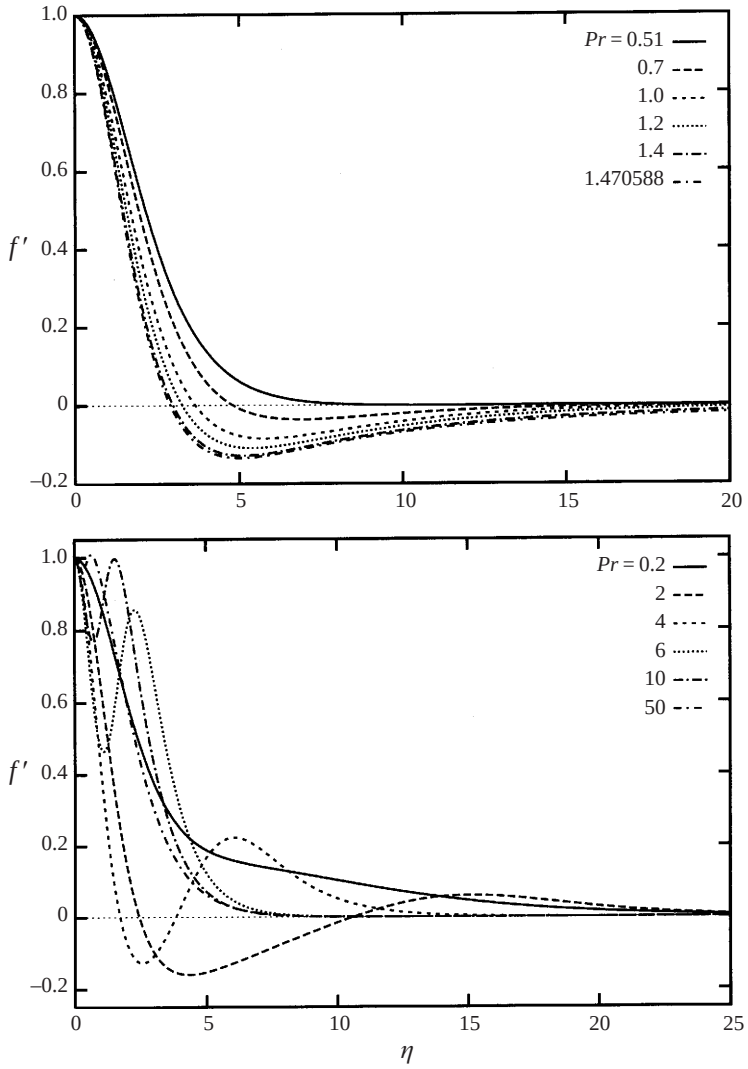

FIGURE 2. Self-similar profiles of the horizontal velocity component in plane buoyant jet flow.

(i.e. non-buoyant) plane jet flow. For $Pr < \frac{1}{2}$ the sign of the temperature disturbance is reversed, see figure 4, which indicates that this mathematical solution does not correspond to the real flow about a horizontal plate as investigated in this work. Rather it is likely, and will be confirmed below, that the far field remains non-buoyant when the Prandtl number drops below the value $\frac{1}{2}$. Thus, the physically acceptable solution is restricted to the Prandtl-number regime $\frac{1}{2} < Pr \leqslant Pr^*$.

2.4. *Solutions of the eigenvalue problem for axisymmetric flow*

For axisymmetric flow ($j = 1$), the set of ordinary differential equations (2.7*a–c*) was solved numerically subject to the boundary conditions (2.9*a*, *b*). As a result, velocity profiles as shown in figure 5 were obtained. In contrast to plane flow, the solution for axisymmetric flow does not show a reversed flow region. Self-similar solutions exist

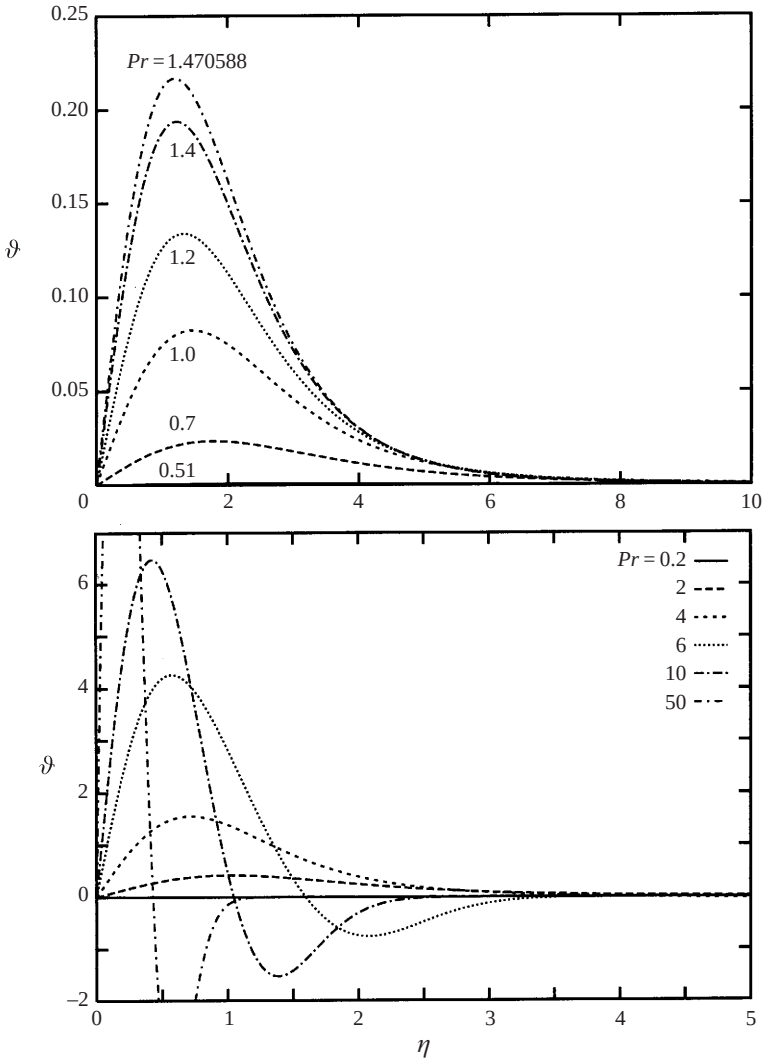

FIGURE 3. Self-similar temperature profiles in plane buoyant jet flow.

for $Pr \geqslant 0.43446$, with $\lambda_1 = \lambda_1(Pr)$ as given in figure 6. The temperature disturbances vanish as $Pr \to 1$, i.e. the solution reduces to the classical solution of the isothermal, non-buoyant axisymmetric ('radial') jet. For $Pr < 1$ the sign of the temperature disturbance is reversed, figure 7, indicating as before in the plane case that the mathematical solution does not correspond to the problem under investigation in this work, see §§ 3 and 5. A solution for $Pr < 0.43446$ has not been found.

For large Prandtl numbers, the viscous boundary layer is much thicker than the thermal boundary layer. Thus the flow field consists of two layers, an inner buoyant layer which drives the flow, and an outer shear layer, see figure 8, $Pr = 50$ and 500.

2.5. *Outer flows induced by horizontal buoyant jets*

The irrotational flow driven by entrainment into the slender jet is described in terms of polar coordinates $r = \hat{r}$, θ. The stream function of the outer flow, ψ_o, is referred to

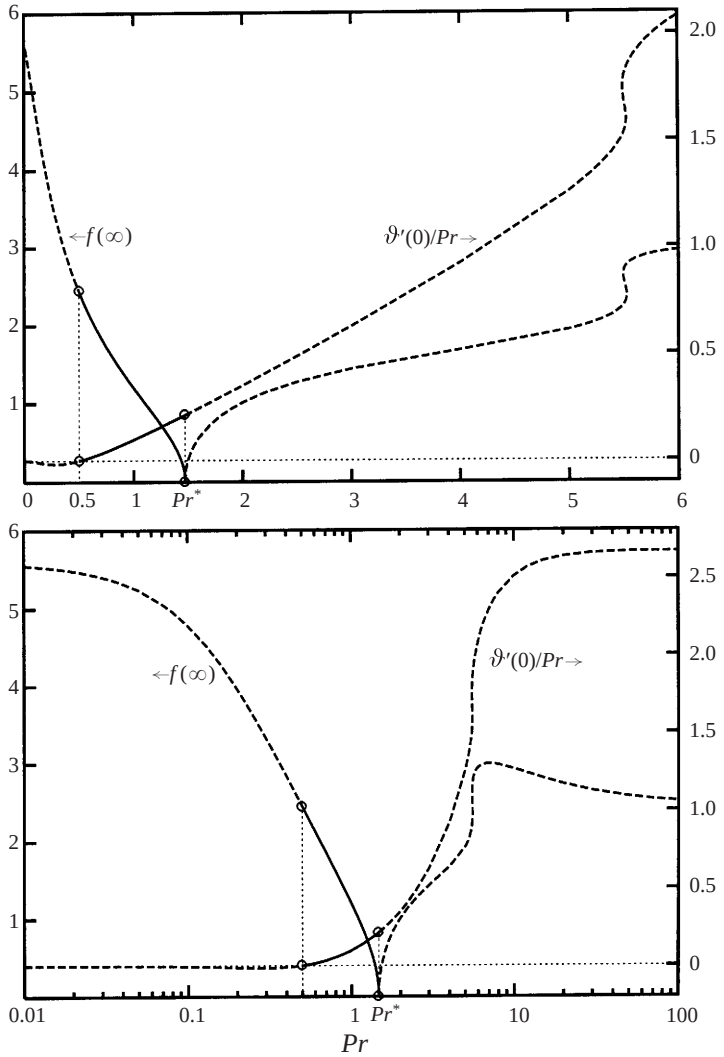

FIGURE 4. $f(\infty)$ (i.e. non-dimensional entrainment rate) and $\vartheta'(0)$ (i.e. non-dimensional heat flux across the plane $y = 0$) for plane buoyant jet flow. Dashed lines: solutions with reversed temperature disturbances.

$L^{1+j}(g\beta\Delta T L)^{1/2}Gr^{-3/10}$. Matching with the inner (jet) flow according to (2.6) requires

$$\psi_o = c^{-1}r^{\lambda_2}f_o(\theta) \tag{2.16}$$

with $f_o(\pi/2) = f(\infty)$, while $f_o(0) = 0$ for reasons of symmetry. Note that $\lambda_2 = \frac{1}{3}$ for plane flow and $\lambda_2 = 2-\lambda_1$ for axisymmetric flow. Introducing (2.16) into the equation of irrotationality and satisfying the boundary conditions for f_o gives

$$f_o = f(\infty)\frac{\sin(\theta/3)}{\sin(\pi/6)} \quad \text{(for plane flow)}, \tag{2.17}$$

where $f(\infty)$ can be taken from figure 4. Apart from the value of the constant $f(\infty)$,

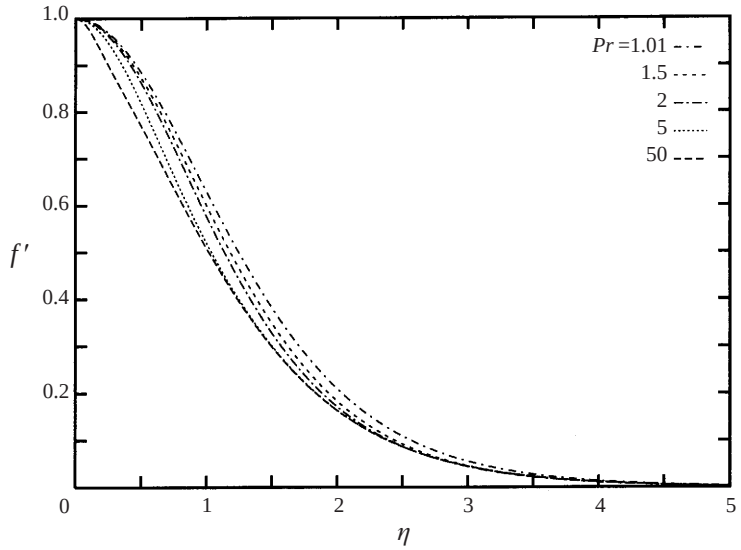

FIGURE 5. Self-similar profiles of the horizontal velocity component for axisymmetric (radial) buoyant jet flow.

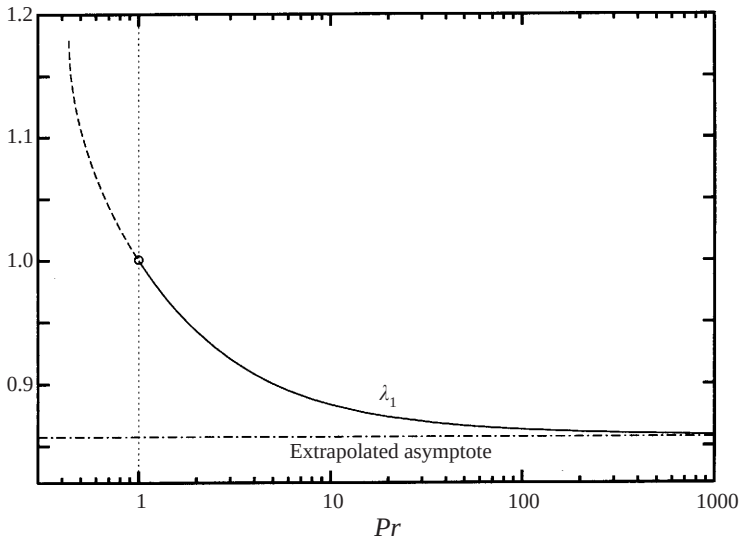

FIGURE 6. The eigenvalue λ_1 as a function of Pr for axisymmetric flow. Dashed line: solutions with reversed temperature disturbances.

(2.17) is in agreement with the classical result for plane laminar jets issuing from a wall (Rubin & Falco 1968; see also Mitsotakis, Schneider & Zauner 1984 for a more precise interpretation). For axisymmetric flow the equation of irrotationality reduces to

$$(1-\chi^2)\frac{\mathrm{d}^2 f_o}{\mathrm{d}\chi^2} + \lambda_2(\lambda_2 - 1) f_o = 0, \tag{2.18}$$

with $\chi = \cos\theta$ and boundary conditions as before in the case of plane flow. The

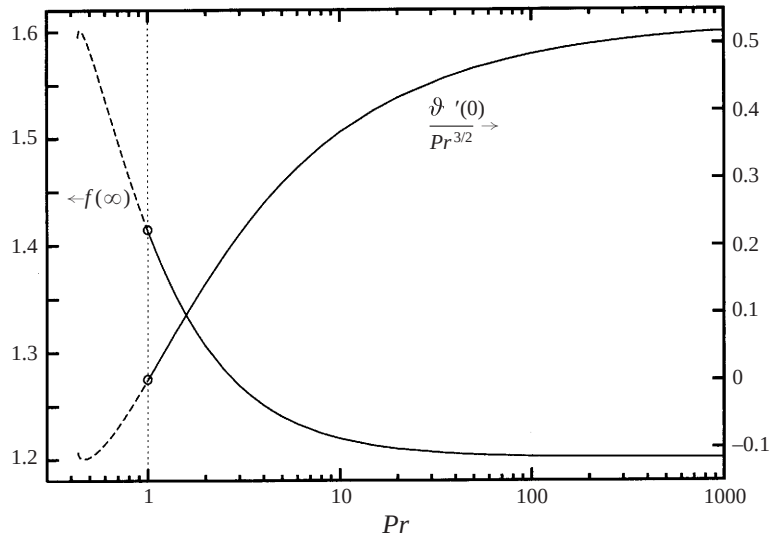

FIGURE 7. $f(\infty)$ (i.e. non-dimensional entrainment) and $\vartheta'(0)$ (i.e. non-dimensional heat flux across the plane $y = 0$) for axisymmetric buoyant jet flow. Dashed lines: solutions with reversed temperature disturbances.

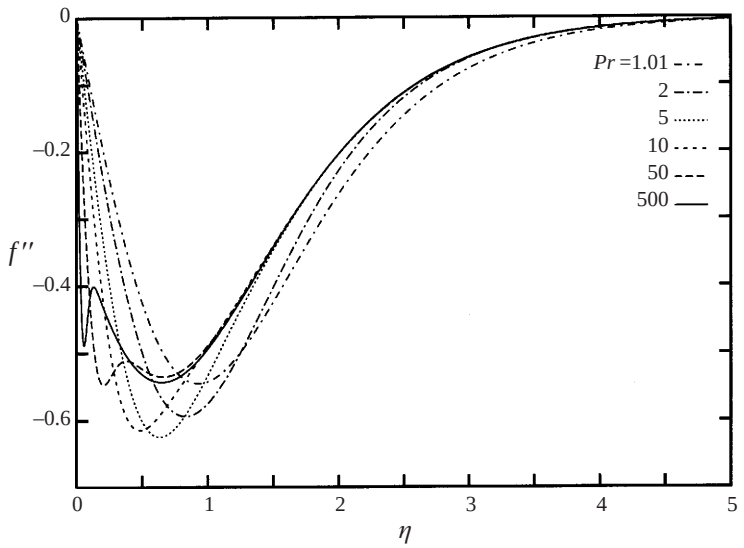

FIGURE 8. Non-dimensional shear stress $f''(\eta)$ for axisymmetric (radial) buoyant jet flow.

solution can be expressed in terms of hypergeometric series (Noshadi 1996), but it appears simpler to solve (2.18) numerically. Results are given in figure 9.

Since heat conduction is negligible outside the boundary-layer region, the induced irrotational flow has the constant temperature of the ambient fluid.

3. Non-buoyant jets

It was shown in the previous section that the buoyancy effects vanish as $Pr \rightarrow \frac{1}{2}$ (for plane flow) or $Pr \rightarrow 1$ (for axisymmetric flow). This suggests (and the comparison

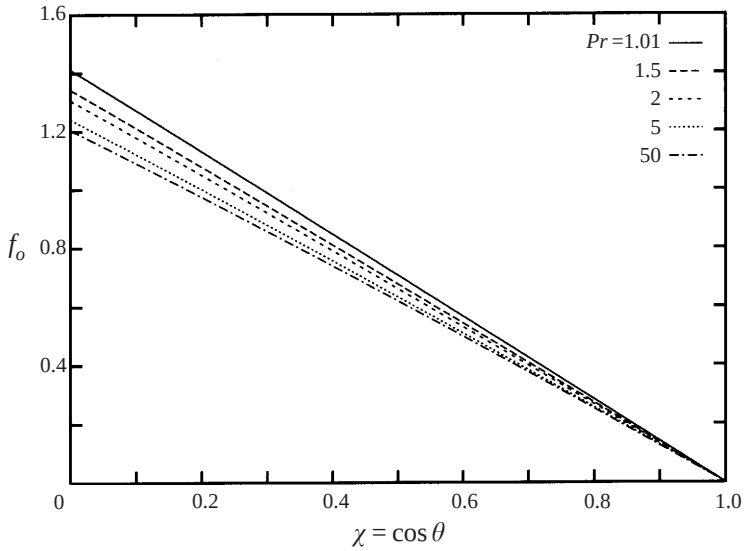

FIGURE 9. Non-dimensional stream function of the inviscid axisymmetric outer flow induced by a horizontal buoyant jet.

with the numerical results to be presented in § 5 will confirm) that the far field is non-buoyant for Prandtl numbers below $\frac{1}{2}$ (plane flow) and 1 (axisymmetric flow), respectively. These cases are now considered.

When the buoyancy term (second term) is dropped in the overall momentum balance (2.10), it follows that

$$\lambda_1 = \frac{2+j}{3}. \tag{3.1}$$

Omitting the buoyancy terms also in the momentum equation (2.7*b*) reduces it such that it can be integrated three times to obtain the result (Schlichting 1979; Rajaratnam 1976; Schetz 1993; Schlichting & Gersten 1997)

$$f = \tanh\tilde{\eta}\ , \quad \tilde{\eta} = \frac{1+2j}{6}\eta. \tag{3.2}$$

Since the equations of momentum and energy are decoupled when buoyancy is neglected, equation (2.8) ceases to be valid for λ_3. Rather λ_3 is an eigenvalue to be determined from solving the energy equation (2.7*c*) subject to the boundary conditions (2.9*a*, *b*). The solution can be expressed in terms of associated Legendre functions, and the eigenvalue is found to be

$$\lambda_3 = -\frac{1+2j}{3}\left(2+\frac{1}{Pr}\right) \tag{3.3}$$

(Noshadi 1996). However, rather than evaluating the Legendre functions it appears preferable to solve the ordinary differential equation (2.7*c*) numerically, making use of the known eigenvalue according to (3.3). Some results will be given in § 5, figures 16 and 19.

4. A self-similar solution of the Navier–Stokes equations

Goldshtik & Shtern (1990) found self-similar solutions to the full Navier–Stokes equations for the axisymmetric natural convection flow originating from a thermal quadrupole. In this section it will be shown that a self-similar solution, with the velocity varying as $1/r$, exists also if the flow is due to a thermal dipole.

It is possible to eliminate the Grashof number from the set of basic equations (1.3), written in spherical polar coordinates, by defining the following scaled non-dimensional variables:

$$r = \hat{r}, \quad \check{v}_r = \hat{v}_r Gr^{1/2}, \quad \check{v}_\theta = \hat{v}_\theta Gr^{1/2}, \quad \check{\Theta} = \hat{\Theta} Gr. \tag{4.1}$$

Then the continuity equation is satisfied by introducing a stream function $\check{\psi}$ according to

$$\check{v}_r = -\frac{1}{r^2 \sin\theta}\frac{\partial \check{\psi}}{\partial \theta}, \quad \check{v}_\theta = \frac{1}{r \sin\theta}\frac{\partial \check{\psi}}{\partial r}, \tag{4.2}$$

and the remaining equations are reduced to ordinary differential equations by means of the substitution

$$\check{\psi} = r\check{f}(\chi), \quad \check{\Theta} = r^{-3}\check{\vartheta}(\chi), \quad \text{with} \quad \chi = \cos\theta. \tag{4.3}$$

Integrating the momentum equation three times, defining a function Q as

$$Q = \int_1^\chi \int_1^\chi \check{\vartheta}\, \mathrm{d}\chi\, \mathrm{d}\chi, \tag{4.4}$$

and making use of the boundary condition $\check{f}(1) = 0$, one eventually obtains

$$(1-\chi^2)\check{f}' + \tfrac{1}{2}\check{f}^2 + 2\chi\check{f} - Q\chi - C(1-\chi)^2 = 0, \tag{4.5a}$$

$$(1-\chi^2)\check{\vartheta}'' + Pr\,(\check{f}\check{\vartheta}' + 3\check{f}'\check{\vartheta}) - 2\chi\check{\vartheta}' + 6\check{\vartheta} = 0. \tag{4.5b}$$

C is a constant of integration that will be determined as a part of the solution. The appropriate boundary conditions are

$$\check{f} = \check{\vartheta} = Q - 2C = 0 \quad \text{at} \quad \chi = 0, \tag{4.6a}$$

$$Q = Q' = 0 \quad \text{and} \quad \check{\vartheta}' = \text{finite} \quad \text{as} \quad \chi \to 1, \tag{4.6b}$$

where $Q(0) = 2C$ follows from $\check{f}''(0) = 0$, expressing symmetry of the radial velocity profile with respect to the horizontal plane, while $Q(1) = Q'(1) = 0$ follows from the definition (4.4). Also, $\check{\vartheta}'(1)$ must be finite to ensure zero heat flux, i.e. $\check{\vartheta}' \sin\theta = 0$, at the axis of symmetry. Numerical solutions for various values of the Prandtl number are given in figure 10.

In the case considered by Goldshtik & Shtern (1990) there is the freedom to choose the value of the temperature disturbance at one boundary, which can be interpreted in terms of different Grashof numbers. In spite of the fact that the set of equations (4.5*a*, *b*) is identical to that solved by Goldshtik & Shtern (1990), there is no free constant in the present problem owing to the different boundary conditions. Therefore the present self-similar solution describes the far field of the natural convection flow due to a heat dipole only for one particular value of the Grashof number. This particular value of the Grashof number depends on the near flow field details. In §5.2 the particular values of Grashof number will be determined by comparing the self-similar far-field solutions with the finite-element solutions of the complete flow field.

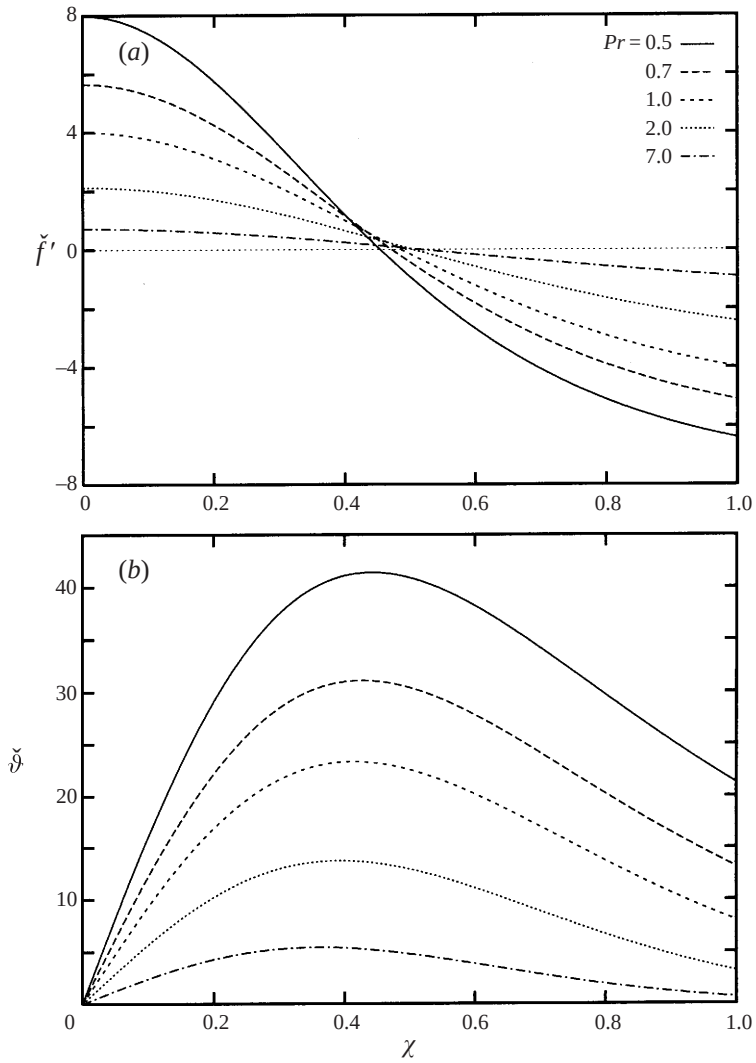

FIGURE 10. (*a*) Radial velocity and (*b*) temperature profiles according to the similarity solution of the Navier–Stokes equations for axisymmetric flow.

5. Comparison with numerical solutions of the Navier–Stokes equations

5.1. *Computational procedure*

The Fluid Dynamics Analysis Package FIDAP, version 6.0 (FIDAP 1991) is applied to compute the far flow field numerically. Thereby, the set of basic equations (1.3) is solved with the method of finite elements, using quadrilateral elements with 9 nodes. To reduce the required memory size and the computation time, the pressure is eliminated from the discretized set of equations using the penalty function approach. If required, the pressure can then be recovered from post-processing the velocity field. Both the velocity and the temperature are approximated using biquadratic interpolation functions.

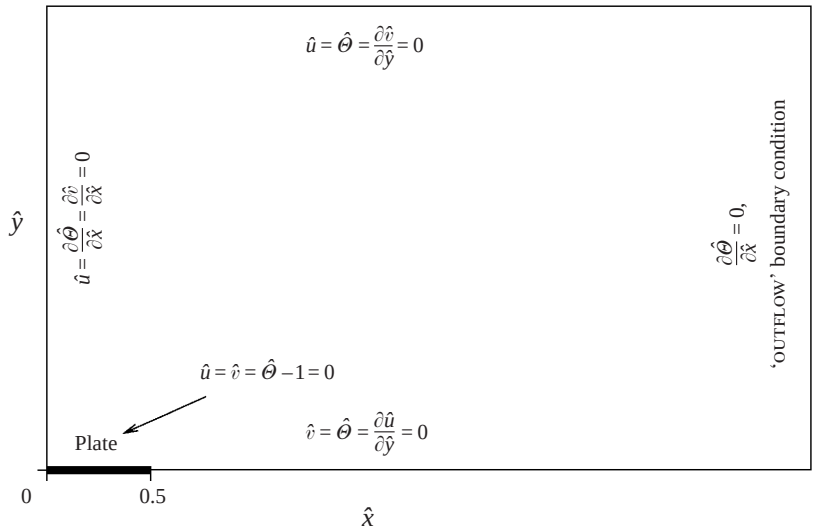

FIGURE 11. Computational domain and boundary conditions.

For the purpose of comparison, the symmetry of the numerically computed flow is assumed to be the same as for the self-similar solutions. Thus the computational domain is restricted to the first quarter of the geometric space as shown in figure 11. (Deviations from this symmetry will be considered in Appendix C.) The distance of the outflow boundary from the origin is chosen such that $Gr_{\hat{x}} = Gr\ \hat{x}^3 > 10^{11}$, while the distance of the upper boundary from the origin is made at least three times the thickness of the boundary layer. The boundary conditions are given in figure 11. The commonly used 'traction-free condition' for the outflow boundary requires both components of the total stress vector to be zero. Since the contribution of the viscous term to the normal stress is rather small, the pressure is forced to be close to zero. This is in conflict, however, with the hydrostatic pressure gradient that remains of importance as the outflow boundary is approached. Therefore, and according to some test computations with various boundary conditions, FIDAP's special 'OUTFLOW' boundary condition (FIDAP 1991) seems to be preferable in this case, as it eliminates the pressure by including the integral of the pressure over the outflow boundary as part of the right-hand-side vector of the system of equations. This integral is updated at each iteration until convergence is attained, i.e. the default criteria for residues and relative errors are met.

5.2. *Discussion of results*

To give an idea of the complete flow field, a streamline plot of plane flow is shown in figure 12. There is a striking resemblance to the classical plane jet flow in the presence of a wall (or symmetry plane) perpendicular to the jet axis (cf. Mitsotakis *et al.* 1984).

An overall momentum balance for the half-space $\hat{x} > 0$ shows that the momentum flow in the far-field jet must be balanced by the hydrostatic pressure distribution in the plane of symmetry near the plate. Thus it is to be expected that bodies with different geometries or sizes, acting as heat dipoles with the same heat flow rate, will generate different far fields. This view is confirmed by the numerical results given in figure 13.

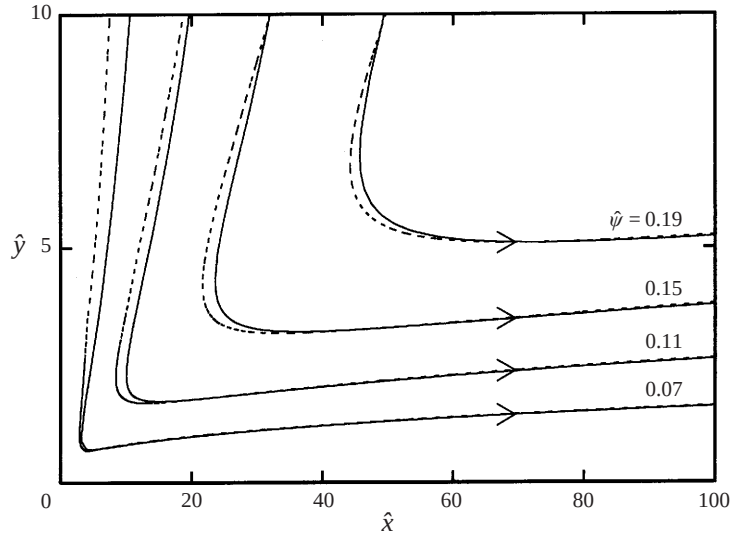

FIGURE 12. Streamlines, plane flow, $Gr = 48\,000$, $Pr = 1$: ——, numerical (FIDAP); - - - -, composite expansion $\psi_+^{(2,1)}$, see Appendix A.

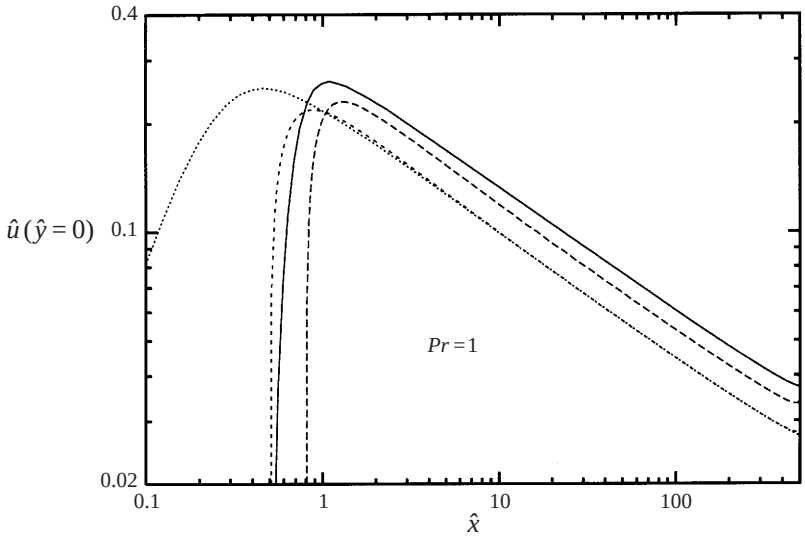

FIGURE 13. Flow velocity in the horizontal plane $\hat{y} = 0$ for various types of heat dipoles with the same heat flow rate (plane flow): ——, horizontal circular cylinder with diameter L and $Gr = 23\,650$; - - - -, horizontal plate with length L and $Gr = 48\,000$; – – –, horizontal plate with length $1.6L$ and $Gr = 38\,950$; ·····, vertical plate with length L and $Gr = 28\,000$.

There is, however, the question of whether buoyancy effects remain of importance as both the velocity and temperature disturbances decay at infinity. Thus we consider values of the local Grashof number

$$Gr_{local} = Gr\ \hat{\Theta}_{max}\ \hat{x}^3, \tag{5.1}$$

where $\hat{\Theta}_{max}$ is the maximum of the temperature disturbance at a fixed value of $\hat{x}$.

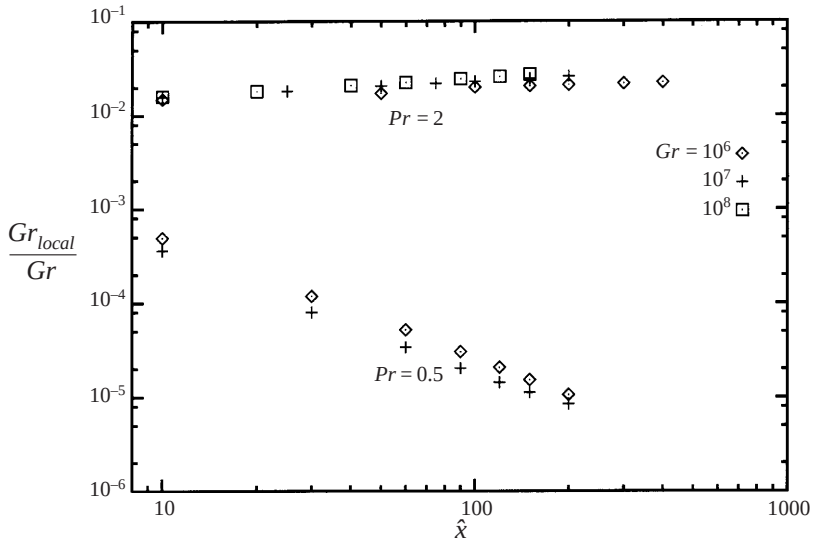

FIGURE 14. Local Grashof number Gr_{local} for large values of the plate Grashof number Gr (axisymmetric flow).

Pr	0.2	0.5	0.7	1.0	1.47	2.0
c (plane flow)	0.79	1.04	1.15	1.28	1.43	—
c (axisymmetric flow)		1.32		1.47		1.94

TABLE 1. Values of the constant c for a horizontal plate of length or diameter L.

Figure 14 gives results for the more interesting case of axisymmetric flow. (For plane flow see Noshadi 1996.) While for $Pr = 2$ the local Grashof number remains large provided the plate Grashof number Gr is large, the local Grashof number decays rapidly for $Pr = 0.5$. This is in accord with the self-similar flows with, and without, buoyancy effects as analysed in §§ 2 and 3, respectively.

To compare the results obtained by various methods, the free constant c in (2.6) is chosen such that at one particular section, i.e. $\hat{x}$ constant, the maximum of the horizontal velocity profile in the jet according to the finite-element solution of the Navier–Stokes equations is equal to that of the self-similar solution of the boundary-layer equations. Then the same scaling is used for comparing temperature profiles, velocity profiles, streamlines etc. at any other section. Some values of the constant c are given in table 1.

5.3. *Comparison of results for plane flow*

In the range $0.5 < Pr \leqslant 1.470588$, the self-similar velocity and temperature profiles of the horizontal buoyant jets are in general agreement with the finite-element solutions of the Navier–Stokes equations, see figure 15. There is, however, some small local disagreement as the finite-element solution predicts a reversed flow region that becomes smaller with increasing distance from the plate. This slight discrepancy seems to be due to the inadequacy of FIDAP's OUTFLOW boundary condition in predicting the reversed flow at the right-hand boundary of the computational domain, while,

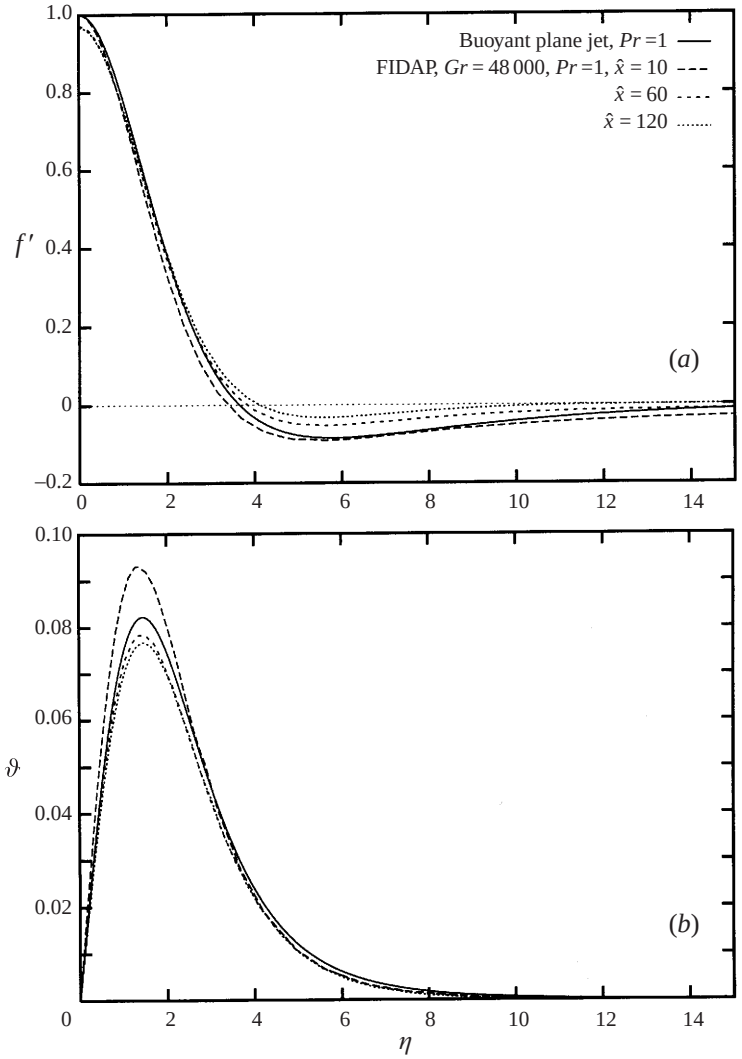

FIGURE 15. Comparison of the self-similar boundary-layer solution for plane, horizontal, buoyant jet flow with the finite-element (FIDAP) solution of the Navier–Stokes equations. (*a*) Profiles of horizontal velocity component; (*b*) temperature profiles.

on the other hand, the analysis of the horizontal buoyant jet is confirmed by a second-order boundary-layer solution (Appendix A, figure 22).

For Prandtl numbers equal to or smaller than $\frac{1}{2}$, the buoyancy effects decay so rapidly with increasing distance from the plate that the far flow field becomes a non-buoyant horizontal jet. Figure 16 shows that the self-similar horizontal velocity and temperature profiles according to the boundary-layer solution of horizontal non-buoyant jets are very close to the corresponding profiles obtained by the finite-element solution of the Navier–Stokes equations.

For Prandtl numbers larger than the critical value 1.470588, finite-element solutions do not show a self-similar structure.

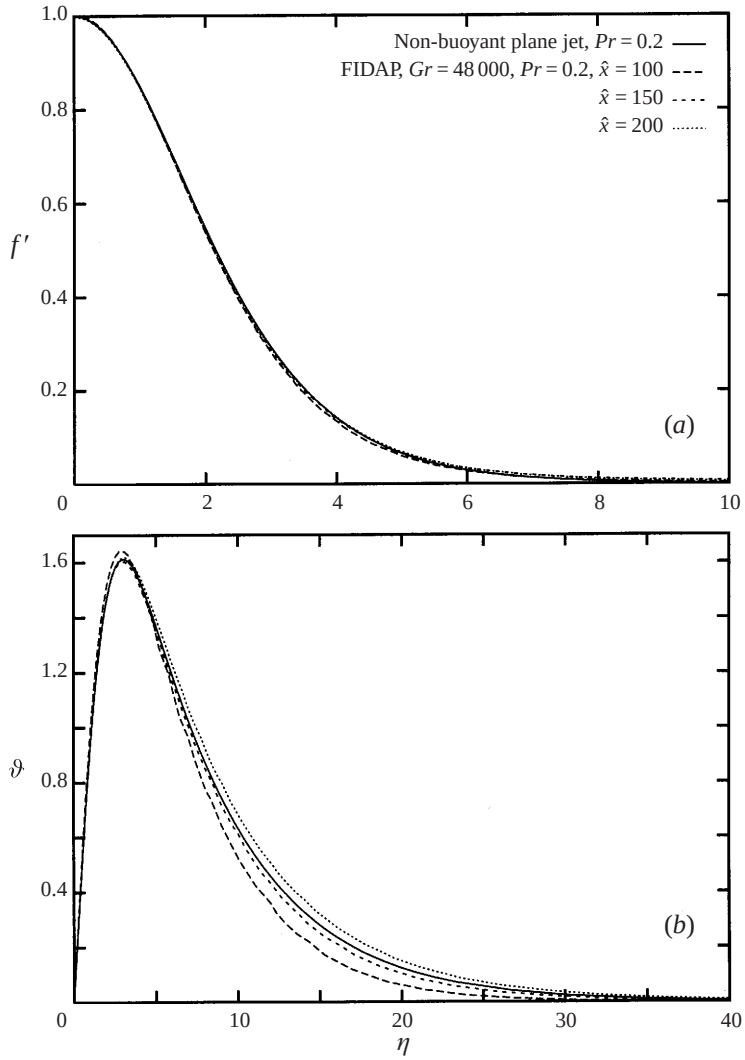

FIGURE 16. As figure 15 but for non-buoyant jet flow.

5.4. *Comparison of results for axisymmetric flow*

From plots similar to figure 13 it is possible to determine the rate of decay of the velocity in the plane of the horizontal plate at large distances from the plate centre. The results are summarized in figure 17. For very large plate Grashof numbers the numerical (FIDAP) results approach the boundary-layer limit, with the limiting eigenvalues depending on the Prandtl number in agreement with the analysis given in §§ 2 and 3. Regarding velocity and temperature profiles, the numerical results given in figures 18 and 19 are in accord with the self-similar boundary-layer solutions for buoyant ($Pr > 1$) and non-buoyant ($Pr < 1$) jets, respectively, provided the plate Grashof number is very large.

For particular, moderately large values of the Grashof number, on the other hand, figure 17 indicates that there are solutions with a velocity decay rate $1 - 2\lambda_1 = -1$, which corresponds to the self-similar solution of the Navier–Stokes equations as

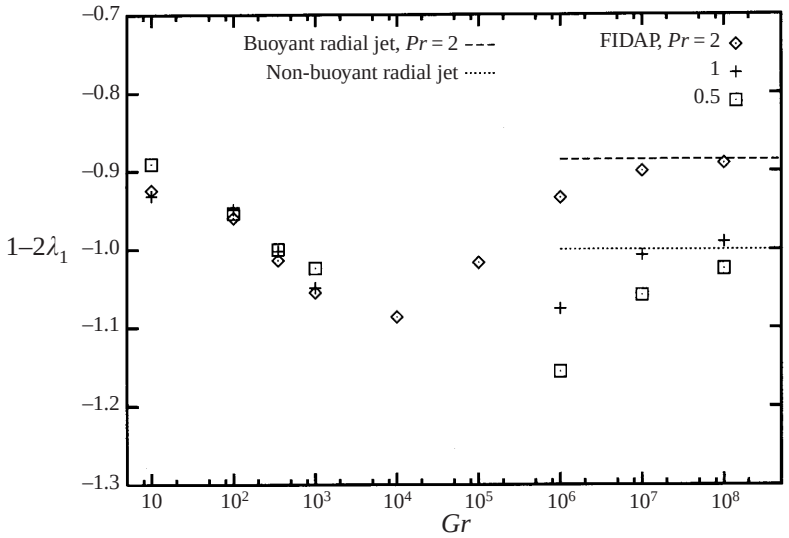

FIGURE 17. Rate of decay of the radial velocity component in the plane of the horizontal plate at large distances from the plate centre: finite-element (FIDAP) solutions of the Navier–Stokes equations compared to limiting values according to boundary-layer theory (axisymmetric flow).

discussed in §4. These particular values of the Grashof number depend on the Prandtl number (see table 2) and on near-field details, especially the shape of the body acting as the heat dipole. To confirm the applicability of the self-similar solution of the Navier–Stokes equations, comparisons with finite-element solutions were made. A result is given in figure 20.

6. Conclusions

Analytical and numerical solutions have been obtained for natural convection flows at large distances from a body (in particular a finite horizontal plate) acting as a heat dipole, i.e. supplying and withdrawing, respectively, the same amount of heat at the lower and upper surfaces. The results lead to the following conclusions.

The far field depends on details of the flow near the heat dipole, i.e. two different bodies acting as heat dipoles with the same amount of heat flow rate generate different far fields.

For very large values of the Grashof number Gr, the far field resembles a horizontal jet flow.

If the Prandtl number Pr is equal to, or smaller than, $\frac{1}{2}$ and 1, respectively, for plane and axisymmetric flow, buoyancy forces are negligible in the horizontal jet at large distances from the body ('non-buoyant jet flow').

In certain Prandtl-number regimes, i.e. $\frac{1}{2} < Pr \leqslant Pr^* = 1.470588$ for plane and $Pr > 1$ for axisymmetric flow, there is a horizontal buoyant jet flow that can be described by self-similar boundary-layer solutions.

In the plane flow case, the eigenvalues of the self-similar solutions are universal constants that can be obtained from an overall momentum balance, whereas in the axisymmetric case the eigenvalues depend on Pr and have to be determined as part of the solution.

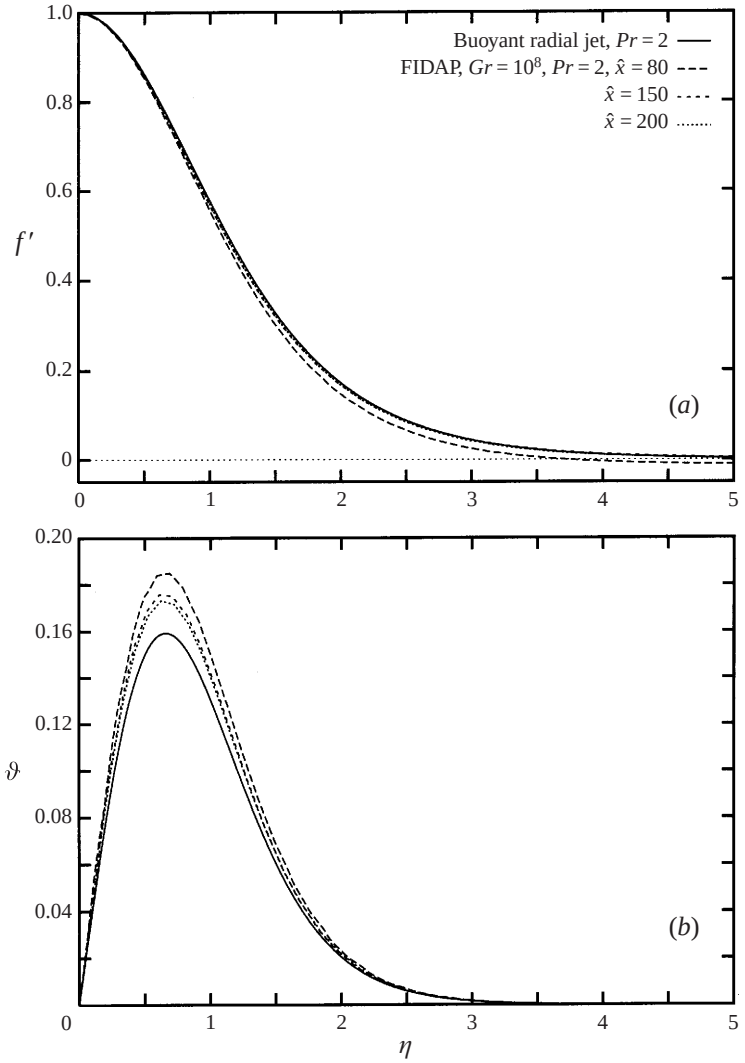

FIGURE 18. Comparison of the self-similar boundary-layer solution for axisymmetric, horizontal, buoyant jet flow with the finite-element (FIDAP) solution of the Navier–Stokes equations. (*a*) Profiles of horizontal velocity component; (*b*) temperature profiles.

For a given Prandtl number *Pr* there is a particular value of the Grashof number *Gr* such that the axisymmetric far field is properly described by a self-similar solution of the Navier–Stokes equations, with the velocity varying as the inverse of the distance from the body (plate) centre.

This work has been supported by the 'Fonds zur Förderung der wissenschaftlichen Forschung in Österreich (FWF)', project No. P9584-TEC. V. Noshadi is grateful to the Iranian Ministry of Culture and Higher Education for financial support. The authors should like to thank the anonymous referees for valuable comments.

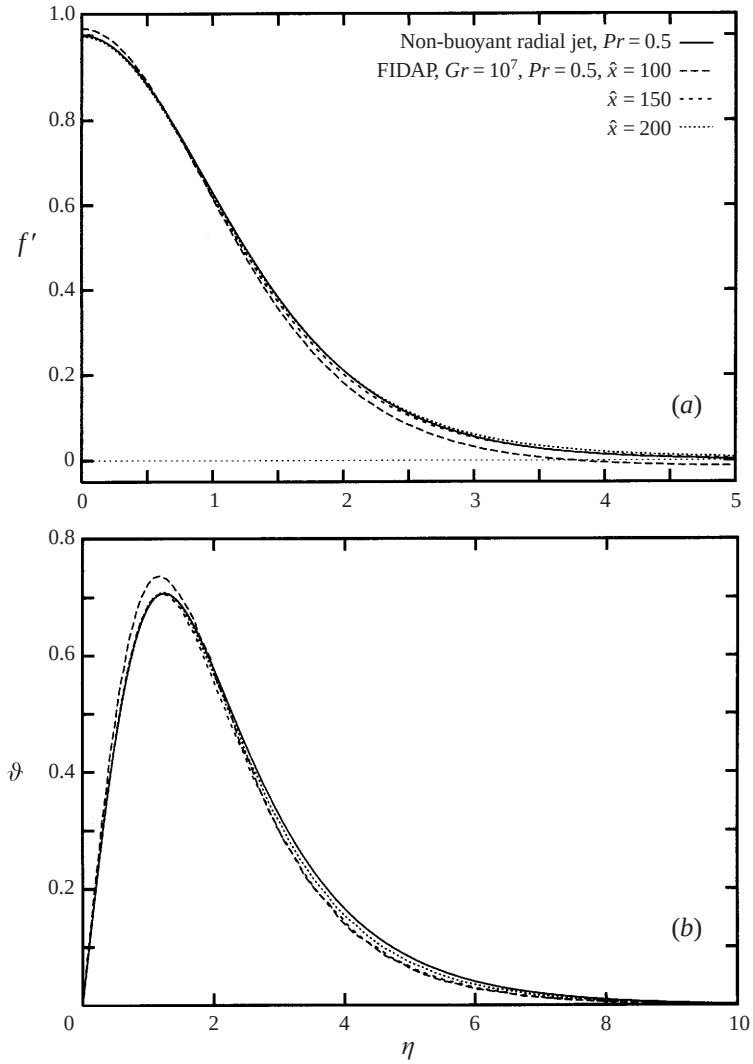

FIGURE 19. As figure 18 but for non-buoyant jet flow.

Pr	0.3	0.5	1.0	2.0	3.0	7.0
Gr	170	360	360	350	220	110

TABLE 2. Values of *Gr*, for which the self-similar solution of the Navier–Stokes equations describes the far field of the natural convection flow due to a horizontal circular plate acting as a heat dipole.

Appendix A. Second-order boundary-layer solutions and uniformly valid solutions for plane flow

To derive the second-order boundary-layer equations for plane flow, the continuity equation, the Navier–Stokes equations and the energy equation are written in Cartesian coordinates using the non-dimensionalization (2.4*a*, *b*). By introducing the stream function ψ according to (2.5) and eliminating the pressure from the Navier–Stokes

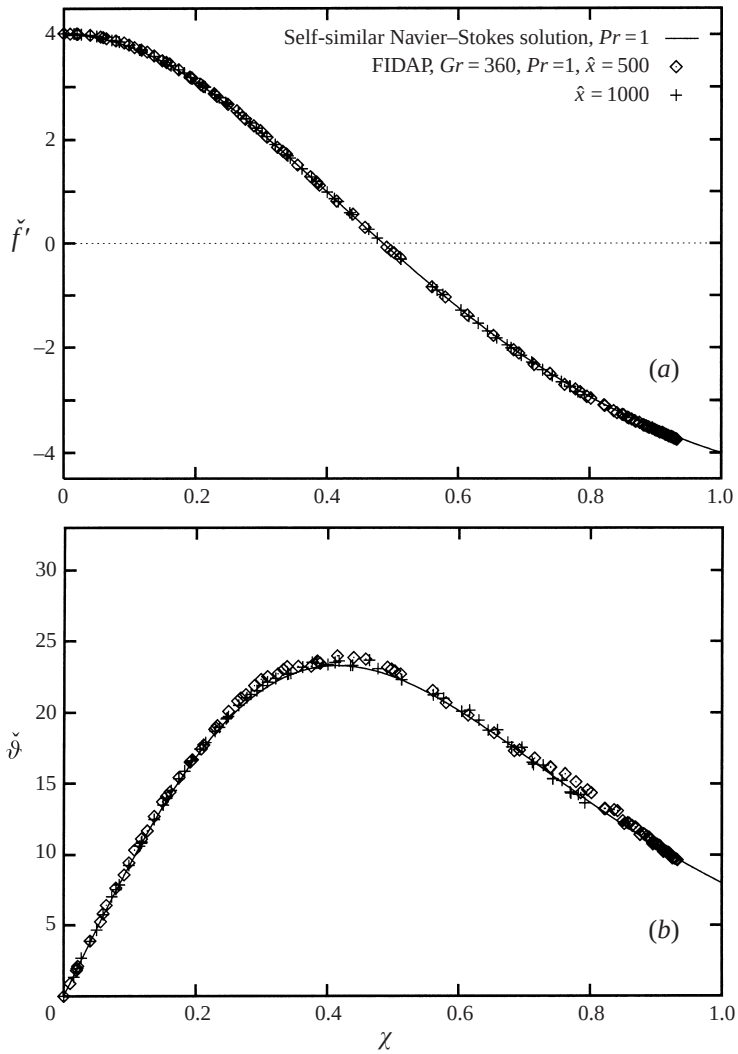

FIGURE 20. Comparison of the self-similar solution with the finite-element (FIDAP) solution of the Navier–Stokes equations for axisymmetric flow. (*a*) Radial velocity component; (*b*) temperature.

equations by differentiating, the set of basic equations transforms to

$$\psi_y\psi_{yyx} - \psi_x\psi_{yyy} + Gr^{-2/5}(\psi_y\psi_{xxx} - \psi_x\psi_{yxx}) = \psi_{yyyy} + Gr^{-4/5}\psi_{xxxx} + 2Gr^{-2/5}\psi_{yyxx} + \Theta_x, \tag{A 1a}$$

$$\psi_y\Theta_x - \psi_x\Theta_y = \frac{1}{Pr}(Gr^{-2/5}\Theta_{xx} + \Theta_{yy}). \tag{A 1b}$$

For $Gr \gg 1$, the inner expansions are

$$\psi = \psi_i = \psi_1 + Gr^{-1/5}\psi_2 + \cdots, \tag{A 2a}$$

$$\Theta = \Theta_i = \Theta_1 + Gr^{-1/5}\Theta_2 + \cdots. \tag{A 2b}$$

The first-order inner expansion has already been considered in § 2, with ψ and Θ representing ψ_1 and Θ_1, respectively, in the present notation. By keeping only the second-order terms, the following set of second-order boundary-layer equations is obtained:

$$\psi_{1y}\psi_{2yyx} - \psi_{1x}\psi_{2yyy} + \psi_{1yyx}\psi_{2y} - \psi_{1yyy}\psi_{2x} = \psi_{2yyyy} + \Theta_{2x}, \tag{A 3a}$$

$$\psi_{1y}\Theta_{2x} - \psi_{1x}\Theta_{2y} + \Theta_{1x}\psi_{2y} - \Theta_{1y}\psi_{2x} = \frac{1}{Pr}\Theta_{2yy}. \tag{A 3b}$$

Introducing f_2 and ϑ_2 with

$$\psi_2 = x^{\lambda_i} f_2(\eta), \quad \Theta_2 = c^{-4} x^{\lambda_i - 5/3}\vartheta_2(\eta) \quad (\lambda_i = \text{const}), \tag{A 4}$$

where c is the same constant as in (2.6), substituting into (A 3*a*, *b*) and integrating once, the boundary-layer equations are reduced to the following set of ordinary differential equations:

$$3f_2''' + ff_2'' + 3f'f_2' = 3q_2 + 2\eta\vartheta_2, \tag{A 5a}$$

$$\frac{3}{Pr}\vartheta_2'' + f\vartheta_2' + 5f'\vartheta_2 = -4\vartheta f_2', \tag{A 5b}$$

where q_2 is defined as

$$q_2 = \int_\infty^\eta \vartheta_2 \mathrm{d}\eta. \tag{A 6}$$

The two-term inner expansion (A 2*a*) is required to match the one-term outer expansion, which is available from (2.16) and (2.17). Applying Van Dyke's matching principle (Van Dyke 1975) gives

$$\lambda_i = 0 \tag{A 7}$$

and

$$f_2(\eta)|_{\eta\to\infty} = -\tfrac{1}{3} f(\infty)\cot\left(\tfrac{1}{6}\pi\right)\eta \tag{A 8}$$

or, in a more convenient form,

$$f_2'(\infty) = -\tfrac{1}{3} f(\infty)\cot\left(\tfrac{1}{6}\pi\right), \tag{A 9}$$

where $f(\infty)$ can be taken from figure 4. With the matching condition (A 9) supplemented by the boundary conditions

$$f_2 = f_2'' = \vartheta_2 = 0 \quad \text{at} \quad \eta = 0, \tag{A 10a}$$

$$\vartheta_2 = 0 \quad \text{as} \quad \eta \to \infty, \tag{A 10b}$$

equations (A 5*a*, *b*) and (A 6) were solved numerically. The solution for $Pr = 1$ is shown in figure 21.

To obtain uniformly valid solutions, two different rules of composition are available (Van Dyke 1975). Whether the additive or the multiplicative composition is preferable depends, in the present problem, on the number of terms to be included. Based on first-order inner and outer expansions, the multiplicative composition $\psi_\times^{(1,1)}$ appears preferable, as the additive composition fails to satisfy exactly the symmetry condition at the Y-axis. However, when the second-order terms of the inner expansion are taken into account, the multiplicative composition breaks down as the common part of the inner and outer expansions vanishes for certain values of the spatial coordinates (Schneider 1973, 1978). Thus, the additive rule is applied in the latter case

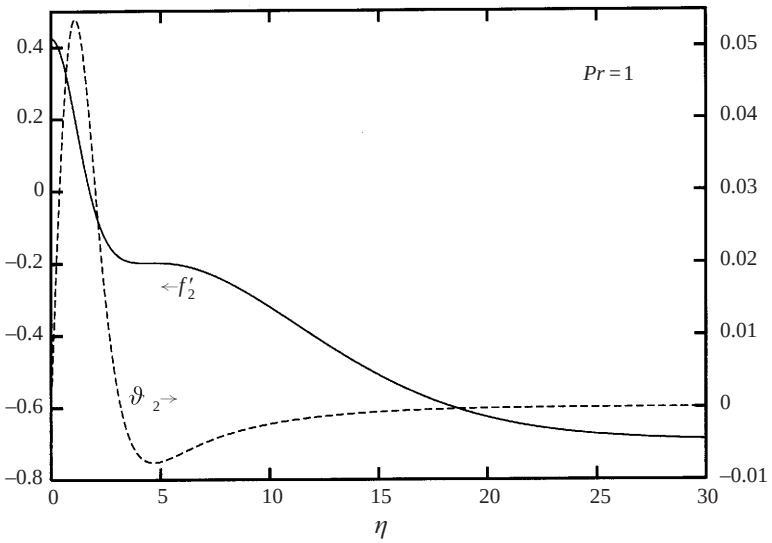

FIGURE 21. Second-order horizontal velocity and temperature profiles for plane buoyant jet flow.

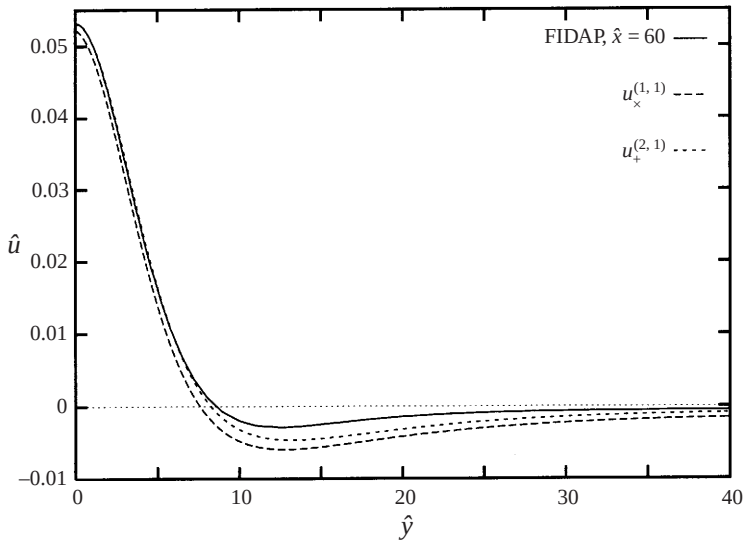

FIGURE 22. Profiles of the horizontal velocity component according to the composite expansions $u_\times^{(1,1)}$ and $u_+^{(2,1)}$ in comparison to the finite-element (FIDAP) solution. Plane flow, $Gr = 48\,000$, $Pr = 1$.

to obtain $\psi_+^{(2,1)}$, see figure 12. Uniformly valid solutions for the horizontal velocity components, $u_\times^{(1,1)}$ and $u_+^{(2,1)}$, are derived from the stream-function solutions, $\psi_\times^{(1,1)}$ and $\psi_+^{(2,1)}$, respectively. A comparison with the numerical solution of the Navier–Stokes equations is given in figure 22.

Appendix B. Asymptotic behaviour of horizontal buoyant jets

To analyse the singularity at the critical Prandtl number, $Pr^* = 1.470588$, in the plane flow case, asymptotic expansions are performed for $\eta \to \infty$. If $Pr \neq Pr^*$, i.e. $f(\infty) = f_\infty = \text{const} \neq 0$, the asymptotic expansions

$$q = C_1 \exp\left(-\tfrac{1}{3} Pr f_\infty \eta\right) + \cdots, \tag{B 1a}$$

$$f' = \exp\left(-\tfrac{1}{3} f_\infty \eta\right) \left\{ \tfrac{2}{3} C_1 \left(\tfrac{1}{3} f_\infty (1 - Pr)\right)^{-2} \right.$$
$$\left. \left[1 - \left(1 - \tfrac{1}{3} f_\infty (1 - Pr)\eta\right) \exp\left(\tfrac{1}{3} f_\infty (1 - Pr)\eta\right)\right] + C_2 \right\} + \cdots \tag{B 1b}$$

satisfy (2.14*a–c*) and the boundary conditions (2.15*a*, *b*). The decaying behaviour of f' as $\eta \to \infty$ is as follows:

$$Pr < 1 \text{ and } Pr \neq \tfrac{1}{2} \quad : \quad f' \sim \eta \exp\left(-\tfrac{1}{3} Pr f_\infty \eta\right), \tag{B 2a}$$

$$1 < Pr \text{ and } Pr \neq Pr^* \quad : \quad f' \sim \exp\left(-\tfrac{1}{3} f_\infty \eta\right), \tag{B 2b}$$

$$Pr = \tfrac{1}{2} \quad : \quad f' \sim \exp\left(-\tfrac{1}{3} f_\infty \eta\right), \tag{B 2c}$$

$$Pr = 1 \quad : \quad f' \sim \eta^2 \exp\left(-\tfrac{1}{3} f_\infty \eta\right). \tag{B 2d}$$

The exponential decay, however, changes to an algebraic one when the critical value of the Prandtl number, $Pr = Pr^*$, is approached. Introducing the asymptotic expansions

$$f \sim F_1 \eta^{-\gamma} + \cdots, \quad q \sim Q_1 \eta^{-\delta} + \cdots \tag{B 3a,b}$$

into (2.14*a–c*) and making use of the boundary conditions (2.15*a*, *b*), the coefficients and exponents of the first-order terms are determined as

$$F_1 = \frac{10}{Pr}, \qquad \gamma = 1, \tag{B 4a}$$

$$Q_1 = -\frac{10}{Pr}\left(\frac{5}{Pr} - 3\right), \qquad \delta = 4. \tag{B 4b}$$

Appendix C. Numerical investigations of symmetry and stability

To verify the assumption of symmetry of the flow field with respect to the X-axis and to study the stability of the jets, both steady-state and transient computations were performed for the half-space, i.e. covering the positive part of the X-axis and the whole Y-axis. FIDAP's version 7.6 with 4-node quadrilateral elements was used. For the boundary conditions see figure 11, with the symmetry condition at the X-axis omitted, of course. Furthermore, the OUTFLOW boundary condition was replaced by the conventional traction-free condition as it turned out that using the OUTFLOW boundary condition for transient computations can lead to unrealistic recirculatory flow regions that grow indefinitely with increasing time.

Provided the net amount of heat transferred from the plate to the surrounding fluid is zero, the laminar steady-state computations for plane flow produce a numerically stable solution with some small deviations of the jet axis from the horizontal, see figure 23. If, however, the heat flow at the upper surface is reduced slightly, e.g. by 0.02%, the jet bends upward as shown in figure 24. For somewhat larger, yet still small, differences (e.g. 0.03%) in the heat supplied at the upper and lower

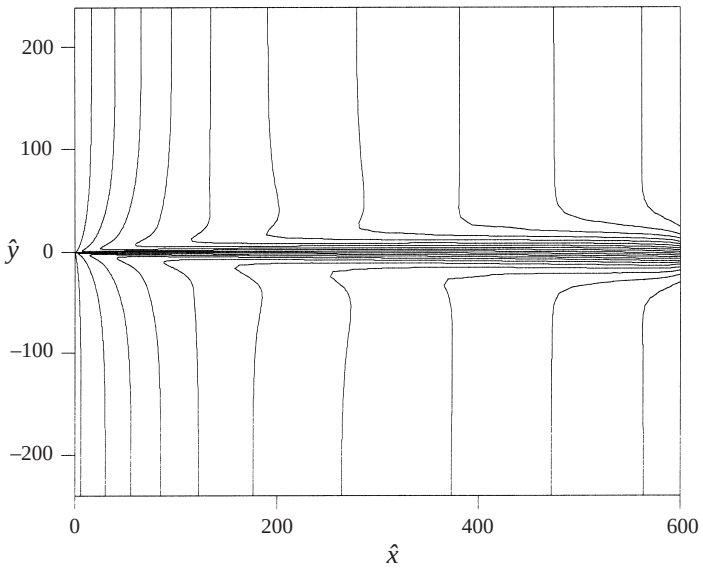

FIGURE 23. Streamline contour plots from steady-state computations for plane flow. $Pr = 1$, $Gr = 10^5$, zero net heat supply.

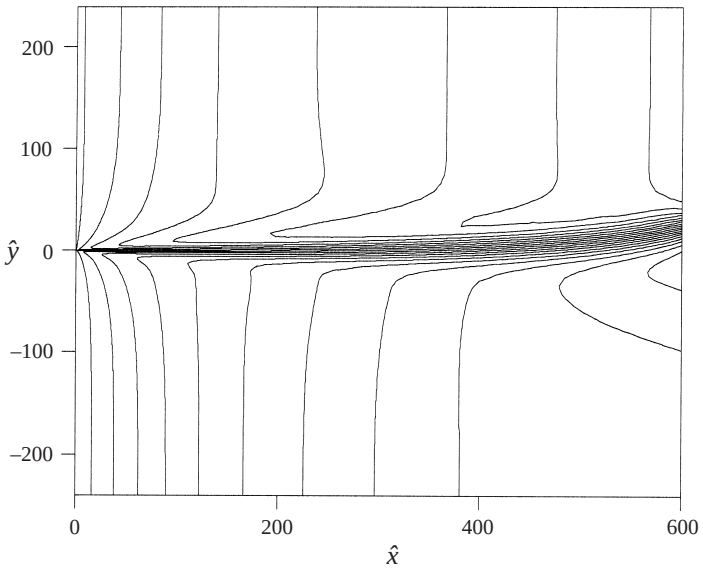

FIGURE 24. Streamline contour plots from steady-state computations for plane flow, $Pr = 1$, $Gr = 10^5$. The prescribed heat flow at the upper side of the plate is 0.02% smaller than that at the lower side.

surfaces, respectively, the flow structure changes to such an extent that the present computations become obsolete.

To study the stability of the plane buoyant jets, transient computations were performed for $Pr = 1$ and various values of the plate Grashof number. Each transient

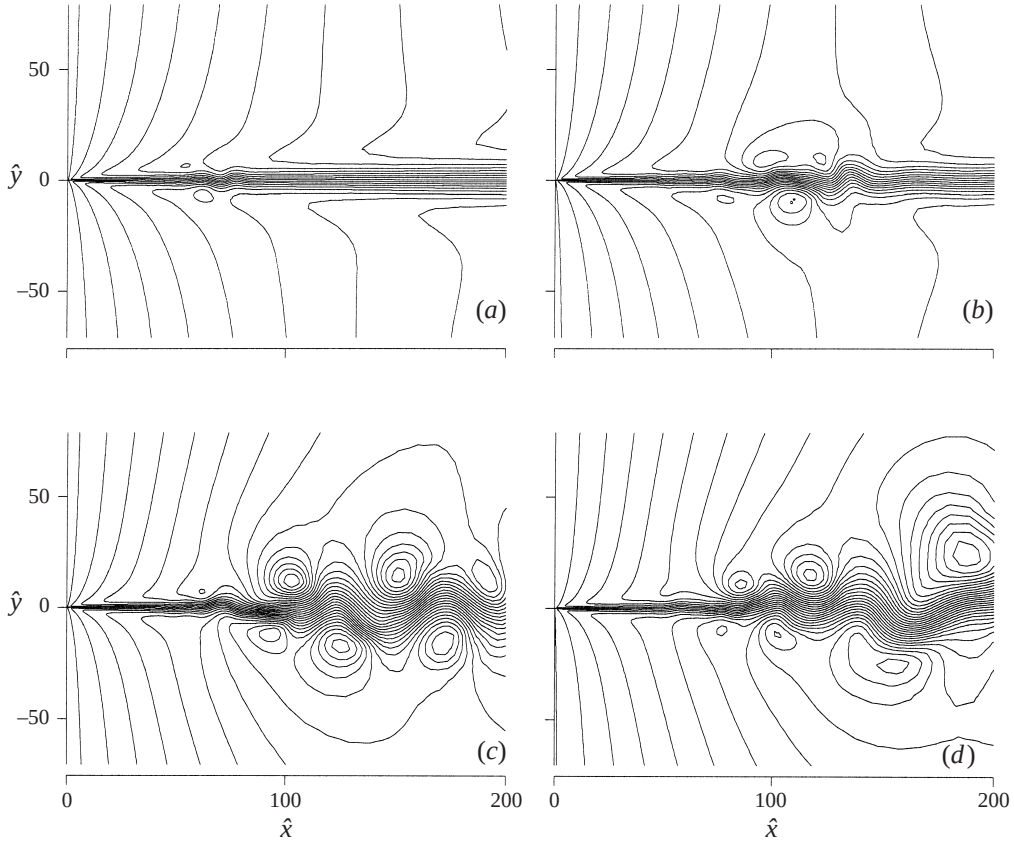

FIGURE 25. Streamline contour plots from transient computations for plane flow, $Pr = 1$, $Gr = 10^5$. (*a*) $\hat{t} = 1500$, (*b*) $\hat{t} = 3000$, (*c*) $\hat{t} = 6000$ and (*d*) $\hat{t} = 9000$.

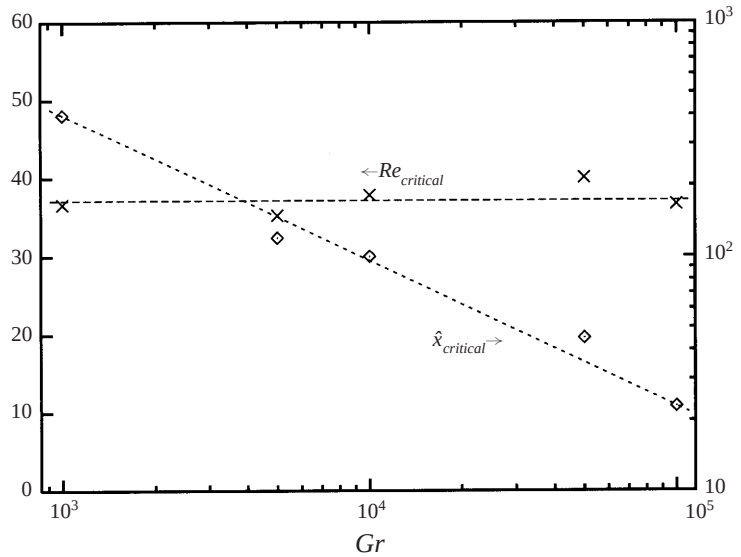

FIGURE 26. Position of, and local Reynolds number at, the critical cross-section, where the instabilities originate, as a function of the plate Grashof number. Plane flow, $Pr = 1$.

computation starts with the result of the corresponding steady-state computation as initial solution. After some time, instabilities appear at a certain distance from the plate. With increasing time, the instabilities grow and propagate in the downstream direction, see figure 25. Here the dimensionless time is defined as

$$\hat{t} = t\left(\frac{g\beta\Delta T}{L}\right)^{1/2}. \tag{C 1}$$

With increasing plate Grashof number, the critical distance $\hat{x}_{critical}$, where the instabilities originate, decrease as shown in figure 26. However, the local Reynolds number,

$$Re = \hat{u}_{max}\ \hat{y}_{max/2}\ Gr^{1/2}, \tag{C 2}$$

at the critical section is nearly independent of Gr and approximately equal to 40, see also figure 26. Here $\hat{u}_{max}$ is the maximum value of the axial velocity component at the cross-section, and $\hat{y}_{max/2}$ is the value of the lateral coordinate where $\hat{u} = \frac{1}{2}\hat{u}_{max}$.

REFERENCES

Ascher, U., Christiansen, J. & Russel, R. D. 1981 Collocation software for boundary-value ODEs. *ACM Trans. MATH. Software* **7**, 209–222.

Barenblatt, G. I. 1979 *Similarity, Self-Similarity, and Intermediate Asymptotics*. Consultants Bureau, Plenum.

Brown, S. N. & Stewartson, K. 1965 On similarity solutions of the boundary-layer equations with algebraic decay. *J. Fluid Mech.* **23**, 673–687.

FIDAP 1991 *Theoretical Manual*, Revision 6.0. Fluid Dynamics International.

Gebhart, B., Jaluria, Y., Mahajan, R. L. & Sammakia, B. 1988 *Buoyancy-Induced Flows and Transport*. Hemisphere.

Gersten, K. & Herwig, H. 1992 *Strömungsmechanik; Grundlagen der Impuls-, Wärme- und Stoffübertragung aus asymptotischer Sicht*. Vieweg.

Gill, W. N., Zeh, D. W. & Del Casal, E. 1965 Free convection on a horizontal plate. *Z. Angew. Math. Phys.* **16**, 539–541.

Goldshtik, M., Hussain, F. & Shtern, V. 1991 Symmetry breaking in vortex-source and Jeffery–Hamel flows. *J. Fluid Mech.* **232**, 521–566.

Goldshtik, M. A. & Shtern, V. N. 1990 Free convection near a thermal quadrupole. *Intl. J. Heat Mass Transfer* **33**, 1475–1483.

Mitsotakis, K., Schneider, W. & Zauner, E. 1984 Second-order boundary-layer theory of laminar jet flows. *Acta Mech.* **53**, 115–123.

Noshadi, V. 1996 Natural convection flows due to heat dipoles. PhD thesis, Technical University of Vienna.

Rajaratnam, N. 1976 *Turbulent Jets*. Elsevier.

Rubin, S. G. & Falco, R. 1968 Plane laminar jet. *AIAA J.* **6**, 186–187.

Schetz, J. A. 1993 *Boundary Layer Analysis*. Prentice-Hall.

Schlichting, H. 1979 *Boundary-Layer Theory*, 7th edn. McGraw-Hill.

Schlichting, H. & Gersten, K. 1997 *Grenzschicht-Theorie*, 9. Aufl. Springer.

Schneider, W. 1973 A note on a breakdown of the multiplicative composition of inner and outer expansions. *J. Fluid Mech.* **59**, 785–789.

Schneider, W. 1978 *Mathematische Methoden der Strömungsmechanik*. Vieweg.

Stewartson, K. 1958 On the free convection from a horizontal plate. *Z. Angew. Math. Phys.* **9a**, 276–282.

Van Dyke, M. 1975 *Perturbation Methods in Fluid Mechanics*, Annotated Edn. Parabolic.